Improving the molecular spin qubit performance in multivariate zirconium MOF hybrids by mechanochemical dilution and fullerene encapsulation

Lucija Vujević,[†] Bahar Karadeniz,[*,†] Nikola Cindro,[‡] Andraž Krajnc,[¶] Gregor Mali,[¶] Stanislav M. Avdoshenko,[§] Alexey A. Popov,[§] Dijana Žilić,[*,†] Krunoslav Užarević,[*,†] and Marina Kveder[*,†]

†*Ruđer Bošković Institute, Bijenička cesta 54, 10000 Zagreb, Croatia.*
‡*Department of Chemistry, University of Zagreb, 10000 Zagreb, Croatia.*
¶*National Institute of Chemistry, Hajdrihova 19, SI-1001 Ljubljana, Slovenia.*
§*Leibniz IFW Dresden, Helmholtzstrasse 20, D-01069 Dresden, Germany.*

Received April 27, 2023; E-mail: bahar.karadeniz@irb.hr; dijana.zilic@irb.hr; krunoslav.uzarevic@irb.hr; kveder@irb.hr

Abstract: Enlarging the quantum coherence times and gaining control over quantum effects in real systems are fundamental for developing of quantum technologies. Molecular electron spin qubits are particularly promising candidates for the realization of quantum information processing due to their modularity and tunability, but there is a constant search for tools to increase their quantum coherence times. Here we present how mechanochemical dilution of active spin qubits in the diamagnetic zirconium-MOF matrix, in synergy with controlled encapsulation of fullerene guest, results in a significant increase in relaxation times and better qubit performances of the moderately porous MOF qubit array candidate. 10% diluted copper(II)-porphyrins as potential molecular spin qubits were incorporated in polymorphic PCN-223 and MOF-525. Spin properties of this hybrid molecular spin qubit frameworks were studied by continuous-wave and pulse electron spin resonance/electron paramagnetic resonance (ESR/EPR) spectroscopy, showing that both spin-lattice and phase memory electron spin relaxation times, T_1 and T_m, respectively, increased by the encapsulation of fullerene molecules into the MOF matrix. Specifically, PCN-223 with a larger filling of fullerene shows better performance in both relaxation times compared with the previously surpassing MOF-525 molecular spin qubit framework.

Introduction

A fundamental step towards the development of quantum technologies is building a qubit, a quantum bit that can exist in a coherent superposition state, unlike the classical bit that can possess only two states, 0 and 1.[1] Among different ways of qubit realization, electron spin in molecular magnetic compounds, where the spin originates from the organic radical, transition metal ion or lanthanide, is particularly promising technology due to the facile manipulation of the electron quantum states by an electromagnetic irradiation.[2,3] The main prerequisite for building a quantum device is the entanglement of qubits to achieve a state that is not the simple product of individual qubits. The inclusion of molecular spin qubits into the specifically tailored environment enables the study of the effect of spatial separation and interactions within the framework on the qubit performance unraveling the role of phonon environment and spin-spin interactions on the operating speed of the qubit (spin-lattice relaxation time rate, $1/T_1$) and on the time limit in which the computation must be performed (phase-memory relaxation time, T_m).[4] A lot of effort is put into suppressing various origins of spin decoherence, such as due to the framework noise and interaction with nearby nuclei.[5] To fully realize the potential of molecular spins for quantum information processing, it is necessary to build structurally well-defined arrays of spatially resolved molecular spins, hence combining improved spin coherence properties with optical or electrical access to their quantum states.[6–8]

Metal-organic frameworks (MOFs)[9,10] assert as an ideal platform for controllable spatial resolution of qubit sites.[4,11] These coordination polymers combine the coordination preferences of the metal cation nodes with different geometry of organic linkers to form a plethora of diverse topologies characterized by permanent porosity, different nature of the interior walls, and approachable metal nodes, not only on the surface but also in the interior of MOF particles. The modularity and tunability of MOFs, particularly MOFs of the fourth generation, made them one of the most investigated material classes today, with many potential application areas.[12,13] In terms of quantum technologies, the variable topologies, periodicity, chemical diversity, and high internal ordering of MOFs provide an ideal and tunable platform for spatial resolution and manipulation of molecular spins, leading towards an emerging class of 3D-qubit array materials.[4] Building such a MOF platform with long coherence time is a demanding task as the spin carriers need to be sufficiently separated from each other, and MOFs inherently carry the magnetic noise of the ligands and guest molecules in the matrix, which leads to rapid decoherence of qubits and usually shorter qubit lifetimes than required for quantum information processing (QIP) or quantum sensing.[14,15] These issues are, however, amendable, and it has been reported that diluting the copper(II)-porphyrin building blocks in highly porous and activated MOFs results in spin coherence detectable up to liquid-nitrogen temperatures, making these materials attractive from the perspective of quantum information science.[4] Therefore, understanding quantum system interactions with its respective environment plays a key step in controlling decoherence processes expressed in terms of T_1 and T_m, (an approximation of spin-spin relaxation time T_2) relaxation times.[16]

A promising class of MOFs for quantum computing are porphyrinic zirconium carboxylate MOFs built from tetratopic porphyrinic ligand, tetrakis(4-carboxyphenyl)porphyrin (TCPP), and hexanuclear or octanuclear oxozirconium(IV) clusters.[17,18] Zirconium carboxylate MOFs[19] are widely researched due to their resistance to water and corrosive atmospheres,[20,21] and framework-stability upon linker removal, leading to increased porosity of the material and larger distancing between the spin carriers.[22,23] Despite zirconium(IV) clusters

and resulting MOFs being diamagnetic, the spin active atom or group can be coordinated in the porphyrin center and efficiently separated by the coordination of the metalloporphyrin with binding carboxylate groups in the MOF structure.[24] Porphyrin MOFs are rare zirconium MOFs displaying more than one topology.[25] For some of the six known topologies, a polymorphic transition is also possible, for example in the case of MOF-525 and PCN-223 (Fig. 1).[26] Freedman group, in their recent proof-of-concept work, exploited cobalt(II) porphyrin molecular magnets diluted in a highly porous hexa-coordinated (on the zirconium cluster) PCN-224 MOF[18] matrix for accomplishing a porous array of clocklike qubits, in order to tackle the issue with magnetic noise of the nuclear-spins rich MOF carrier.[27] The same group showed how the incorporation of spin-active copper(II) porphyrins into the PCN-224 results in porous molecular spin-based qubits with detectable coherence among the highly-concentrated spins in the framework up to 80 K (Fig. 1).[4,28] In this context copper(II) porphyrins, where the copper bears $S = 1/2$ electronic spin, became attractive and extensively studied model systems for spintronic applications while the coherence parameters in terms of T_1 and T_m were investigated using pulse ESR spectroscopy in addition to continuous wave (CW)–ESR.[24,29,30] Not only the molecular spin-based qubits with high porosity and missing linkers, such as PCN-224, are suitable molecular spin qubit candidates. In our recent work, we showed how mechanochemistry[31] provides a controllable pathway to the synthesis of phase-pure twelve-coordinated PCN-223 and MOF-525 polymorphs.[26] By introducing paramagnetic centers (Cu(II), Fe(III), and Mn(II)) in the porphyrin linker, a superhyperfine splitting was observed in CW–ESR, spectra of the more porous MOF-525 polymorph, whereas the same feature was less pronounced in PCN-223 where the nearest distance between the paramagnetic centers is 1.07 nm.[26] The observed phenomenon denoted these materials as potential candidates for applications in spintronics.

Here presented study is focused on the modulation of copper(II)-porphyrin qubit properties in the MOF-525 and PCN-223 polymorphic pair by dilution of the spin carriers in the MOF structure. We are particularly interested to see how the controllable mechanochemical incorporation[32] of a strong electron-acceptor guest such as C_{60} fullerene within the voids and channels of formed molecular spin based qubit will be reflected on the coherence of the spin arrays in the robust non-activated MOF samples. The results show that the introduction of fullerene changes not only the electron structure of the hybrids, but also that the selectivity of framework formation turns exclusively towards hard-to-obtain PCN-223 polymorph, with the fullerene residing in triangular channels along the crystallographic c axis. For the purpose of this study we prepared two fulleretic molecular spin based qubit PCN-223 frameworks with different amount of fullerene. The analyses of CW–ESR spectra unravel magneto-structural characteristics of copper-porphyrin qubit environment including the local symmetry of the copper center in terms of g and hyperfine A tensors for both diluted-spin molecular spin based qubit. Beside direct measuring of spin-relaxation times, other pulsed ESR experiments were performed, such as HYSCORE and Rabi oscillations, in order to gain the relevant information about the interactions with far distant and remote nuclei. The introduction of fullerene to the voids of molecular spin based qubit significantly increases the spin-spin coherence, promoting the least successful molecular spin based qubit to the one with the longest T_m.

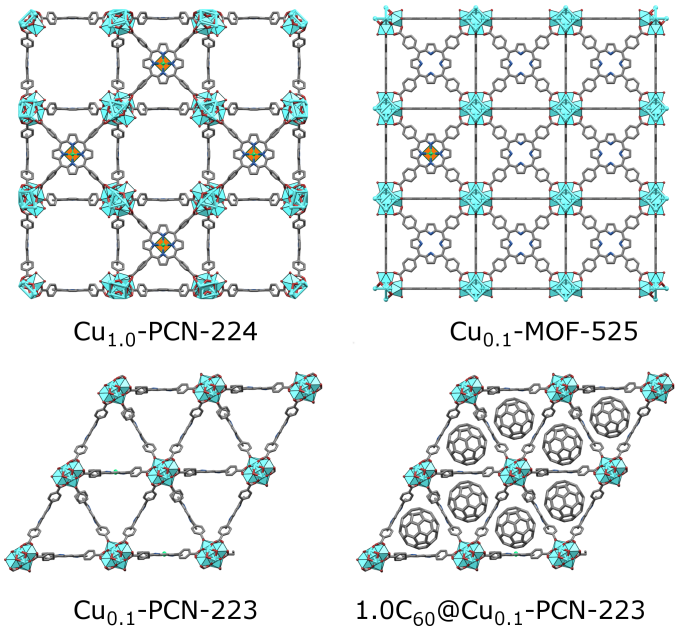

Figure 1. Porphyrinic Zr-MOFs considered for spintronics application; six-coordinated PCN-224 with low population of linkers allowed for dense Cu(II) spin-arrays (orange-green polyhedra in the center of porphyrin moiety).[4] MOF-525 and PCN-223 involved in this study are twelve-coordinated, with a dense population of mixed TCPP linkers involving 10 percent of Cu(II)-TCPP. Introduction of fullerene steers the formation exclusively towards PCN-223 framework, with the fullerene populating the voids of the MOF.

Results and discussion

Synthesis and CW/pulse ESR studies of 12-connected porphyrinic zirconium MOF polymorphs, Cu-MOF-525 (cubic, *ftw*), Cu-PCN-223 (hexagonal, *shp*) and their composites, are presented. Copper(II) ratio in the porphyrin centers of the synthesized MOFs was diluted to 10% copper(II) as the copper(II)–copper(II) interactions cause line broadening in CW–ESR and destroy electron spin coherence in pulse ESR.

Synthesis

Synthesis and controlled topology transformation of metallated and metal-free MOF-525 and PCN-223 by mechanochemistry has been recently reported by our group.[26] Diluted $Cu_{0.1}$-MOF-525 and $Cu_{0.1}$-PCN-223 frameworks were synthesized in the same manner by mixing the desired ratio of CuTCPP and TCPP ligands. Here, whereas the mechanochemical formation could not completely control the distribution of the CuTCPP in the framework, the ESR analyses showed efficient separation of copper centers in the formed multivariate MOFs (please see section CW–ESR spectroscopy below). Controlled amount of fullerene C_{60} (20 and 100%) was successfully encapsulated into $Cu_{0.1}$-PCN-223 using the one-pot LAG MOF formation.[32] Noteworthy, even with the reaction conditions[26] that would previously exclusively afford the cubic *ftw*-$Cu_{0.1}$-MOF-525 polymorph, the presence of C_{60} in reaction mixture driven the formation exclusively towards hexagonal *shp*-C_{60}@$Cu_{0.1}$-PCN-223 with different amount of fullerene in the channels. The washing of the crude milling product was almost colorless, indicating, together with the FTIR and PXRD analyses, that the guest was included in

the framework in its entirety. Based on these results, C_{60} thus acted as a template providing the C_{60}@$Cu_{0.1}$-PCN-223 hybrid, and fulleretic hybrid of MOF-525 was not yielded in any of the attempts despite this kinetic phase being much more common in conventional mechanochemical synthesis.[26] Tentatively, the arrangement of the linkers and channel size of PCN-223 polymorph is more suitable for encapsulation of C_{60}. Similar effect of C_{60} template on tuning the cavity size of multi-porphyrin macrocycles has been reported previously.[33]

Synthesized MOFs and MOF composites are phase-pure and highly crystalline, and no fullerene is visible in products after mild toluene and DMF washing (Fig. 2). The disappearance of C_{60} peaks in the PXRD patterns confirms the absence of C_{60} crystals on the surface of MOF composites. PXRD data also provide a qualitative measure of the reach of encapsulation of C_{60} within the PCN-223 framework. The intensity of the low angle peak, $2\theta = 4.80$, decreases due to the modified electron density in the MOF cage as a result of loading C_{60} in the channels of PCN-223 framework,[32,34] which is also corroborated here by DFT. Calculated PXRD data closely matched the experimentally observed PXRD data, supporting the reduction of the low-angle peak intensity, which is the effect of guest inclusion into the cage(Fig. 2).

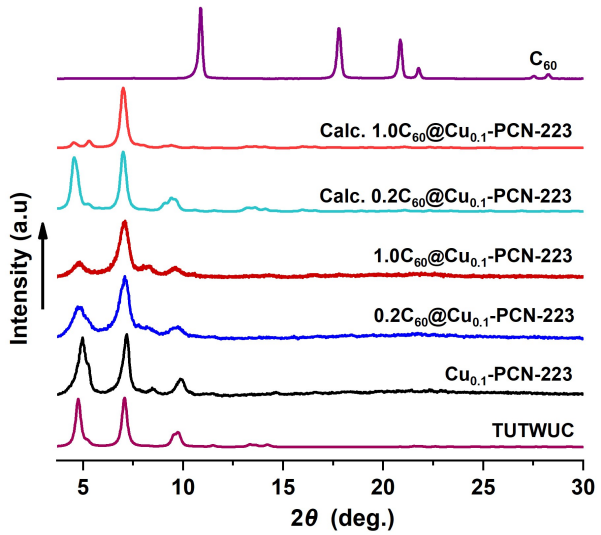

Figure 2. PXRD data for $Cu_{0.1}$-PCN-223 and the C_{60}@$Cu_{0.1}$-PCN-223 composites vs PXRD data for PCN-223 simulated from the single crystal diffraction data (Cambridge Crystallographic Data Centre (CCDC) code: TUTWUC).

DFT study

The system size allows a comprehensive DFT study (DFT/PAW/PBE-D, see SI for computational details) of the stability and dynamics of the PCN-223 framework with C_{60} molecules inside. The PCN-223 framework is rather spacious, and after full optimization, no significant change in the C–C bond parameters of the C_{60} fullerene itself could be observed. The calculations also reveal a lack of significant affinity of the fullerene molecules toward the MOF framework, and the C_{60} molecules tend to stay in the middle of the voids. Unlike the fullerene situated in the ZIF-8 framework where fullerenes are locked and immobilized in the respective voids,[32] fullerenes can freely move along the 1D channel of PCN-223. Within the channel, molecules appear to be well isolated from other parallel channels, although the distance between the closest molecules from the neighboring channels is roughly 6 Å. At the same time, the distance among the C_{60} molecules within a single channel is 8 Å, which undermines the possibility of significant electronic interaction between them. High-density fillings would be required to provide significant intermolecular interaction among the fullerenes within the channel. Further investigation of the system using the DFTB/MD method reveals that molecules can freely rotate on-site (Fig. 3(a)). Fig. 3(a) shows the time-averaged trajectory of the carbon cage atoms along the 100 picosecond trajectory while the vibrational density of states are shown in Fig. 3(b). The time-averaging smooths out continuous molecular motion along with the principal components of rotations. Within the channel, such a rotation would undoubtedly lead to a sizeable disorder. The aforementioned dense packing might partially prevent such intense rotations.

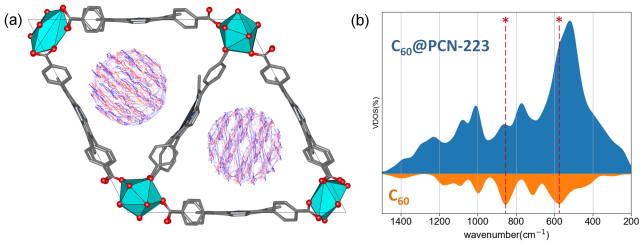

Figure 3. (a) Superposition of time-averaged snapshots for C_{60} within a 100 ps time-window of C_{60}@PCN-223 dynamics at DFTB level of theory. (b) MD recovered the total and projected vibrational density of states for C_{60}@PCN-223 and C_{60}, where asterisks mark the most profound contribution by C_{60} in the total VDOS.

FTIR-ATR spectroscopy

FTIR-ATR data of $Cu_{0.1}$-MOF-525, $Cu_{0.1}$-PCN-223, and (20% and 100%), C_{60}@$Cu_{0.1}$-PCN-223 are consistent with their counterparts in the literature.[26] The formation of a new vibrational peak at 526 cm^{-1} with a slight shift in the spectrum of (20% and 100%) C_{60}@$Cu_{0.1}$-PCN-223 is clearly assigned to the most dominant vibration signal of pristine C_{60}, at 523 cm^{-1}, proving the incorporation of C_{60} into the framework while the other vibration peaks of pristine C_{60} overlap with the framework features (Fig. S1).

NMR spectroscopy

The results of solid-state NMR spectroscopy are presented in Fig. 4 while peaks assignment was performed from the analysis of CPMAS and HETCOR spectra (Fig. S2, Fig. S3). In specific, ^{1}H and ^{13}C MAS recorded for 1.0C_{60}@$Cu_{1.0}$-PCN-223 indicates the NMR signal corresponding to formamide additive implying that the solvent is still present within the pores of the network. The signal of ^{13}C nuclei of C_{60} in the C_{60}@$Cu_{0.1}$-PCN-223, appearing at ca. 138 ppm, is narrow, suggesting that fullerene is quite mobile inside the MOF channels. Any stronger anisotropic interaction with proximal paramagnetic copper centers is thus motionally averaged out. In the sodalite zeolitic-imidazolate-framework-8, fullerene was completely immobilized in the discrete voids of the framework, and its inclusion led to stiffening of the framework and increased resistance towards the radiation.[32] The ^{13}C MAS NMR spectra of C_{60}@$Cu_{0.1}$-PCN-223 in the region between 125 ppm and 135 ppm and at about 145 ppm, where the signals of the linkers appear, indicates that the incorporation of C_{60} into the pores of PCN-223 leads to a similar stiffening effect.

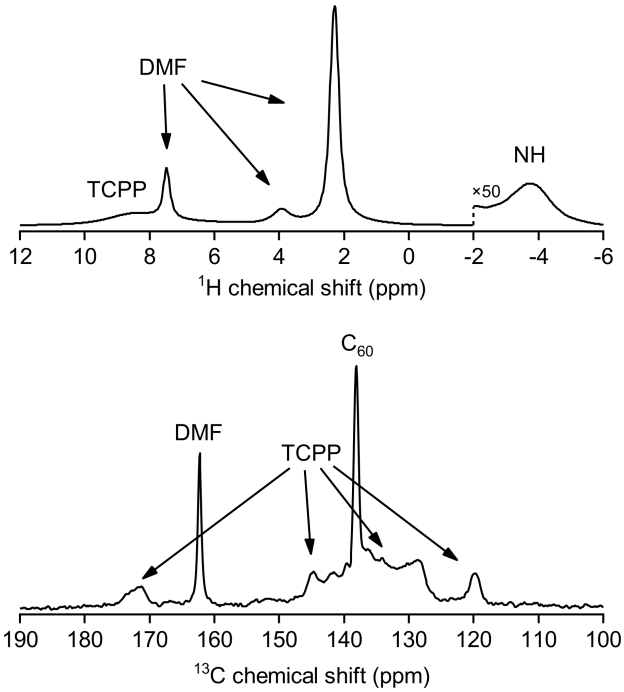

Figure 4. ^{1}H and ^{13}C MAS NMR spectra recorded for 1.0C$_{60}$@Cu$_{0.1}$-PCN-223 sample at 300 K. The signals from dimethylformamide (DMF) solvent, TCPP ligand and fullerene (C$_{60}$) are indicated on the spectra.

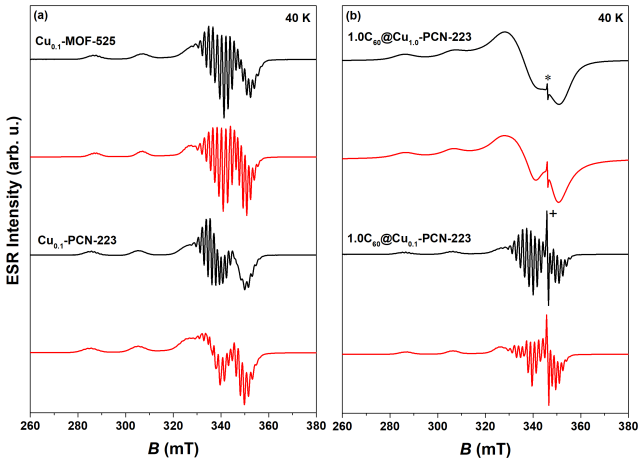

Figure 5. Experimental (black) and simulated CW–ESR spectra (red) of various MOFs recorded at 40 K: (a) Cu$_{0.1}$-MOF-525 and Cu$_{0.1}$-PCN-223, (b) 1.0C$_{60}$@Cu$_{1.0}$-PCN-223 and 1.0C$_{60}$@Cu$_{0.1}$-PCN-223. Asterisk in the figure indicates the fullerene signal at $g \approx 2.003$ while "+" denotes truncation of the fullerene peak. Parameters of the simulated spectra are reported in Table S1.

CW–ESR spectroscopy

CW–ESR spectra of various MOFs recorded at 40 K showing axial symmetry are presented in Fig. 5. It can be noticed that both Cu$_{0.1}$-MOF-525 and Cu$_{0.1}$-PCN-223 exhibit typical CW–ESR spectra of the diluted copper porphyrin monomers (Fig. 5a).[29,35] The strong hyperfine coupling of the unpaired electron spin with the copper nuclear magnetic moment ($I = 3/2$) results in four lines from which three are resolved in the low-field part of the spectrum. In comparison with the previously reported ESR spectra, which did not reflect the interaction with four nitrogen atoms from the porphyrin macrocycle in the first derivation of the absorption ESR spectra due to the high copper concentration (100% Cu),[26] here presented data exhibit strong modulation of the high-field part of the spectrum (Fig. 5a). This superhyperfine interaction in the ESR spectra of a sample with lower concentration of copper ions (10% Cu) provides evidence of the capability of mechanochemical procedures to dilute metal ions in the molecular framework in a largely controllable manner.

The experimental spectra were simulated using EasySpin software[36] assuming axial symmetry of **g** tensor and **A** hyperfine tensor while all four nitrogen atoms in the porphyrin ring were assumed to be equivalent.[37] In specific, the tensor components $g_\parallel$ and $A_\parallel$ correspond to the orientation perpendicular to the porphyrin plane while $g_\perp$ and $A_\perp$ represent planar, plane orientation.[4] In the interaction of the copper electron spin ($S = 1/2$) with the copper nucleus spin ($I_{Cu} = 3/2$) the same hyperfine coupling for natural-abundance mixture of copper isotopes (^{63}Cu and ^{65}Cu) was assumed.[35] Therefore, the following spin-Hamiltonian for copper electron spin was used:

$$H_{Cu} = \mu_B B g S + S A_{Cu} I_{Cu} + S A_N I_N \qquad (1)$$

where B is external magnetic field while the constant μ_B is Bohr magneton. The parameters obtained from the simulations are given in Table S1 and are consistent with the data reported in the literature.[4,38] In specific, the spectra exhibit $g_\parallel > g_\perp > g_e$ indicative of the $d_{x^2-y^2}$ copper electron spin ground state. No essential difference of **g**-tensor values in Cu$_{0.1}$-PCN-223 and Cu$_{0.1}$-MOF-525 indicates no difference in their respective orbital angular momentum contributions. Similarly, hyperfine/superhyperfine tensor differences are within the experimental variability of data. In addition, the tetrahedral distortion of the square planar copper geometry[39] estimated from the ratio $f = g_\parallel / A_\parallel^{Cu}$ indicates perfect planar geometry which pertains upon the incorporation of fullerene (Table S2). Interestingly, the incorporation of fullerene was successful in PCN-223 but following the same procedure not in MOF-525 and the corresponding CW–ESR spectra of 1.0C$_{60}$@Cu$_{1.0}$-PCN-223 and 1.0C$_{60}$@Cu$_{0.1}$-PCN-223 are presented in Fig. 5b. Fullerene has a weak ESR signal at $g_{C_{60}} \approx 2.002$ due to defects in fullerene structure.[32] This signal is even visible when the structure was loaded with 100% of Cu although the superhyperfine lines could not be resolved due to strong spin-spin interactions between copper cations (Fig. 5b). Due to this fact, the simulation of the experimental spectra was done in terms of a mixture of spin species by combining the spin-Hamiltonian of copper given by Eq. 1 and spin-Hamiltonian of fullerene while assuming $S_{C_{60}} = 1/2$:

$$H_{C_{60}} = \mu_B B g_{C_{60}} S_{C_{60}}. \qquad (2)$$

The simulation parameters[36] and the corresponding spectra are given in Table S1 and Fig. 5b. The obtained data are in accordance with the NMR and DFT studies and the literature stating that encapsulated fullerene is free standing inside the cage and, thus, not affecting the coupling of copper electron spin with the nuclei in the vicinity, albeit affecting dynamics of organic linkers.[32]

Pulse ESR spectroscopy

Two-pulse echo detected field-swept ESR spectra of various MOFs were recorded at 80 K in order to assign the spectral positions for relaxation time measurements in pulsed ESR

experiments (Fig. 6a). Two Cu(II) magnetic field resonances were chosen, which correspond to two principle **g**-tensor values $g_{\parallel} = 2.2$ and $g_{\perp} = 2.06$.[4]

Spin-lattice relaxation time

The electron spin-lattice relaxation times, T_1, of four MOF-samples: $Cu_{0.1}$-PCN-223, $0.2C_{60}$@$Cu_{0.1}$-PCN-223, $1.0C_{60}$@$Cu_{0.1}$-PCN-223 as well as of $Cu_{0.1}$-MOF-525 were measured across temperature range of 5–80 K. The shortest T_1 was detected for $Cu_{0.1}$-PCN-223 which upon loading of the fullerene molecules into the structure presented much longer T_1 values (Fig. 6b). This phenomenon can be noticed in the whole temperature range studied. In specific, the longest T_1 of ca. 6.7 (5.3) ms was measured at 5 K and $g_{\parallel}$ position for $0.2C_{60}$@$Cu_{0.1}$-PCN-223 ($1.0C_{60}$@$Cu_{0.1}$-PCN-223) as compared with the empty $Cu_{0.1}$-PCN-223 which exhibited T_1 of ca. 3.5 ms. Upon heating of the samples to 80 K, T_1 values decreased by three orders of magnitude and converged to the similar T_1 values in the range of 5 μs (Fig. 6b). For all the samples studied T_1 measured at $g_{\parallel}$ was longer than the one at $g_{\perp}$ position by a factor of two at lowest temperatures studied (Fig. S4). Interestingly, at lowest temperatures studied T_1 values of MOF-525 were similar to the values of PCN-223 loaded with fullerene while approached the similar values of other MOFs upon heating up the sample (Fig. S4).

In order to understand the experimental data, three main processes of the spin-lattice relaxation rate, $1/T_1$, could be assumed to transfer the spin excitation energy to the acoustic phonons of a crystal lattice: direct one-phonon process, two-phonon Raman and Orbach-Aminov process.[40] In this context, assuming the Debye type of phonon spectrum, experimental $1/T_1$ values were simulated according to equation[40–42]

$$1/T_1 = aT + b\frac{T^9}{\theta^7}J_8 + c\frac{1}{e^{\Delta/T}-1}, \qquad (3)$$

as shown in Fig. 6b while the best-fit parameters are given in Table S3. The first term describes the one-phonon process and it is important at lowest temperatures studied, when the phonons with high energy are still not excited. The second term is related to the two-phonon Raman process with J_8 denoting the transport integral, which was solved numerically, while θ is Debye temperature. The last term describes Orbach process that is going over excited electronic state of energy Δ.[40,43,44] The observation that for all the compounds studied T_1 measured at the spectral position of $g_{\parallel}$ was longer than the one measured at $g_{\perp}$ can be accounted for the enhanced influence of the direct process at the later than the former principal **g**-tensor axis being perpendicular to the porphyrin plane.

The phenomenon that MOF containing fullerene in the structure exhibited the largest T_1 value points to the different vibrational environment of copper porphyrins in the PCN lattice (Fig. 6b). This observation is in line with the recent report on the inclusion of fullerene in zeolitic-imidazolate framework[32] and here presented findings from FTIR-ATR and SS-NMR, showing that fullerene content affects vibrational properties of three-dimensional MOF framework Figs. S1 and 4. In the presence of fullerene, the vibrational spectrum of the framework is changed in such a way that less low-energy phonons satisfying resonant condition for the direct one-phonon process are accessible for the energy exchange between the spin system and the lattice. Therefore, electron spin relaxation is slowed down, as reflected in increased T_1.

Phase-memory relaxation time

The temperature dependence of the electron-spin phase-memory relaxation times, T_m, of various MOFs is presented in Fig. 6c for $g_{\parallel}$ spectral position. At 5 K, the longest T_m value around 800 ns was detected in $1.0C_{60}$@$Cu_{0.1}$-PCN-223. It can be seen that T_m is affected by the content of fullerene in the structure giving rise to the shortest T_m in $Cu_{0.1}$-PCN-223 (540 ns) whereas $Cu_{0.1}$-MOF-525 featured T_m of 600 ns (Fig. 6c). Upon increasing the temperature above 5 K, T_m exhibited no temperature dependence up to ca. 30 K. Here, spectral diffusion as a temperature independent process can be assumed. Further heating of the samples revealed gradual decrease of T_m according to the Arrhenius type of thermally activated processes with the larger activation energy when the fullerene is present in the MOF structure (Fig. 6c). Since even at 80 K T_m was at least one order of magnitude smaller than T_1 for all the samples studied, it can be concluded that T_m is not T_1 limited.

HYSCORE

It should be mentioned that two-pulse electron spin-echo decay curves for various MOFs presented strong modulation depths in the coherence time decays reflecting specific nuclear spin environment affecting the copper electron spin relaxation (Fig. S5). The phenomenon appeared irrespective of the presence/absence of fullerene. Due to the fact that in the two-pulse echo experiments also the multiples of the nuclear frequencies could contribute in the modulation spectra, 2D-HYSCORE experiment was performed (Fig. 7a). In the (+,+) and (–,–) quadrants one can note the signals from the weakly coupled nuclei appearing on the diagonal at ca. 0.84, 3.7 and 14.4 MHz. The later peak can be assigned unambiguously to the X-band proton Larmor frequency and corresponds to the hyperfine interaction with the remote hydrogen (^{1}H) nuclei. However, the diagonal peak appearing at 3.7 MHz could be of various origin. In specific, the interaction with distant ^{14}N nuclei, which due to the nuclear spin $I = 1$ exhibit non-spherical charge distribution, requires quadrupolar interaction to be taken into account. As a support for this reasoning the low-frequency peak at 0.84 MHz can be noticed and assigned to the remote weakly coupled ^{14}N nucleus close to the cancellation limit when the hyperfine and nuclear Zeeman terms match in one of the electron spin manifolds giving rise to the ^{14}N quadrupolar transitions.[45,46] It has been reported that around 4 MHz a double quantum (DQ) transition of the remote nitrogen can be detected.[46–49] Furthermore, when the interactions of electron spin with more than one ^{14}N takes place, the combination frequency of 3.33 MHz and 9.38 MHz could be observed[50] but also DQ frequency of ^{14}N which exhibits 2DQ peak at ca. 9 MHz at the anti-diagonal in (–,+) and (+,–) quadrants could be noticed.[47] However, Larmor frequency of ^{13}C nucleus appearing at 3.7 MHz at X-band was assigned in the HYSCORE spectra of copper porphyrin nanorings despite the very low abundance of this isotope.[29] As a support for this reasoning, in the ^{13}C enriched sample the splitting of 6 MHz was assigned to ^{13}C hyperfine coupling,[51] the similar splitting that could be measured between [0.84,6.3] MHz and [6,3.84] MHz cross peaks in Fig. 7a. Therefore, since at X-band frequency the contributions of ^{14}N and ^{13}C nuclei are not well separated they should be both considered while unambiguous assignment would require HYSCORE measurement at higher frequency like Q-band. It is interesting to note that the modulation patterns/HYSCORE data are not different for $Cu_{0.1}$-PCN-223 with and without loaded

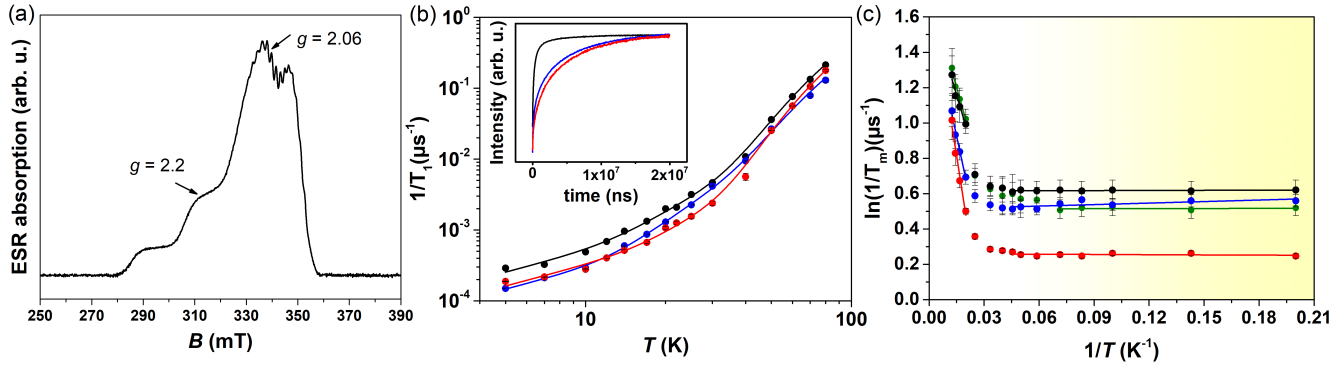

Figure 6. (a) Two-pulse echo detected field-swept ESR spectrum of $Cu_{0.1}$-PCN-223 recorded at T = 80 K. The tensor values $g_{\parallel}$ = 2.2 and $g_{\perp}$ = 2.06 labeled by arrows indicate the magnetic field spectral positions at which spin dynamics was undertaken. (b) Temperature dependence of the electron spin-lattice relaxation rate, $1/T_1$, in $Cu_{0.1}$-PCN-223 (black), $0.2C_{60}$@$Cu_{0.1}$-PCN-223 (blue) and $1.0C_{60}$@$Cu_{0.1}$-PCN-223 (red) measured at $g_{\parallel}$ spectral position. Full lines denote simulations of the experimental data according to the Eq. 3 with the parameters given in Table S3. In the inset to the figure magnetization recovery curves are given in the inversion recovery experiment detected at 5 K. (c) Temperature dependence of the electron-spin phase-memory relaxation time, T_m, in various MOFs at $g_{\parallel}$ spectral position. The best fits according to Arrhenius equation (full line) are indicated. In the temperature interval from 40–80 K the activation energies are: 35±5 K ($Cu_{0.1}$-PCN-223, black), 48±5 K ($0.2C_{60}$@$Cu_{0.1}$-PCN-223, blue), 67±8 K ($1.0C_{60}$@$Cu_{0.1}$-PCN-223, red) and 37±4 K ($Cu_{0.1}$-MOF-525, green).

fullerene in the structure. Relying on the experimental evidence from NMR measurements showing signals from formamide additives in the context of this study the origin of the observed modulation pattern could be assigned to remote nitrogen nuclei from the solvent (more than 0.4 nm away from the copper electron spin) apart from the directly coordinated ones which affect CW–ESR spectra (Fig. 5).

Rabi oscillations

Since paramagnetic MOFs are considered as potential qubits,[52] the nutation experiments were performed at different microwave powers at 20 K as shown in Fig. 7b. Rabi oscillations could be detected for all MOFs studied and exhibited similar behavior. After Fourier transformation of the time domain data (Fig. 7c) the peak centered at ca. 13.5 MHz, independent of the microwave power, is assigned to originate from coherent electron-proton oscillations. Its intensity reaches the maximum when the Larmor frequency of proton spins matches electron nutation frequency.[30] The nutation frequency peak shifts from 9.2 to 16.4 MHz with increasing microwave magnetic field. Linear dependence of the Rabi frequency on the microwave field can be observed (Fig. 7d).

Conclusion

In summary, this study shows how the multivariate metal-organic framework hybrids can be exploited for efficient spatial isolation and controllable manipulation of the molecular spin qubit performance. Mechanochemical processing accomplished through a robust one-pot ball-milling procedure allowed for control over the ratio of active spin copper(II) carriers in the MOF matrix and simultaneous introduction of the controllable amount of fullerene C_{60} guest into the pore-channels of porphyrinic zirconium MOFs with twelve-coordinated oxocluster nodes. The use of C_{60} leads to topological selectivity by governing the formation towards PCN-223 phase, even from reactions that exclusively yield cubic MOF-525 polymorph. Here presented experimental evidence points to the possibility of fine-tuning the electron spin relaxation times via fullerene content in the MOF cavity, where a significant increase in T_1 and T_m is detected in MOF fulleretic hybrids, with coherence times depending on the ratio of the fullerene guest. In this way, even the non-activated and densely coordinated zirconium-porphyrin frameworks become viable molecular spin qubit matrices, where the inferior and least porous $Cu_{0.1}$-PCN-223 candidate becomes the best qubit performer after the fullerene inclusion. Using similar solid-state strategies, we aim to test how altering the spin carrier species and including fullerene and endometallofullerene derivatives in more porous zirconium-porphyrinic MOFs, such as twelve-coordinated MOF-525 and already well-established six-coordinated framework PCN-224, will affect their spintronics properties.

Acknowledgment

This research was supported in part by the Croatian Science Foundation through grant IP-2018-01-3168, by the "Research Cooperability" Program of the Croatian Science Foundation funded by the European Union from the European Social Fund under the Operational Programme Efficient Human Resources 2014-2020, through grant PZS-2019-02-4129, and by the DAAD-MZO bilateral project "New generation of magnetic MOF composites based on controllable confinement of selected endofullerenes". A.K. and G.M. acknowledge the financial support from the Slovenian Research Agency (research core funding No. P1-0021).

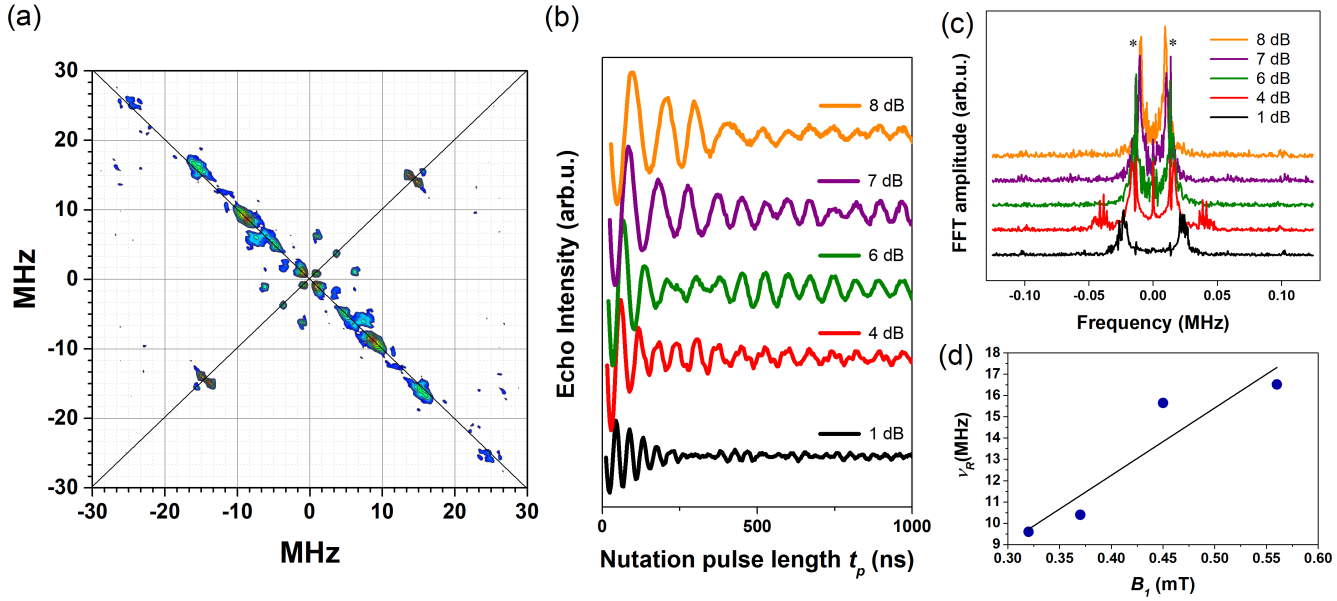

Figure 7. (a) 2D-HYSCORE performed at 5 K and $g_{\|}$ spectral position for $1.0C_{60}$@$Cu_{0.1}$-PCN-223 plotted after data processing. (b) Rabi oscillations recorded for $1.0C_{60}$@$Cu_{0.1}$-PCN-223 at 20 K and $g_{\|}$ spectral position applying various microwave attenuation. c) Fast Fourier transform (FFT) of the Rabi oscillations with asterisk denoting Larmor frequency of proton spins. (d) Linear dependence of the Rabi frequency, ν_R, as a function of the oscillating microwave field, B_1.

References

(1) Atzori, M.; Sessoli, R. The Second Quantum Revolution: Role and Challenges of Molecular Chemistry. *J. Am. Chem. Soc.* **2019**, *141*, 11339–11352.

(2) Gaita-Ariño, A.; Luis, F.; Hill, S.; Coronado, E. Molecular spins for quantum computation. *Nat. Chem* **2019**, *11*, 301–309.

(3) Cronado, E. Molecular magnetism: from chemical design to spin control in molecules, materials and devices. *Nat. Rev. Mater* **2020**, *5*, 87–104.

(4) Yu, C. J.; Krzyaniak, M. D.; Fataftah, M. S.; Wasielewski, M. R.; Freedman, D. F. A concentrated array of copper porphyrin candidate quibts. *Chem. Sci.* **2019**, *10*, 1702–1708.

(5) Graham, M. J.; Zadrozny, J. M.; Fataftah, M. S.; Freedman, D. E. Forging Solid-State Qubit Design Principles in a Molecular Furnace. *Chem. Mater.* **2017**, *29*, 1885–1897.

(6) Andlauer, T.; Vogl, P. Electrically controllable g tensors in quantum dot molecules. *Phys. Rev. B* **2009**, *79*, 045307–045314.

(7) Graham, M. J.; Zadrozny, J. M.; Fataftah, M. S.; Freedman, D. F. Forging Solid-State Qubit Design Principles in a Molecular Furnace. *Chem. Mater.* **2017**, *29*, 1885–1897.

(8) Bayliss, S. L.; Deb, P.; Laorenza, D. W.; Onizhuk, M.; Galli, G.; Freedman, D.; Awschalom, D. Enhancing spin coherence in optically addressable molecular qubits through host-matrix control. *Phys. Rev. X* **2022**, *12*, 031028–031036.

(9) Zhou, H.-C.; Long, J. R.; Yaghi, O. M. *Chem. Rev.* **2012**, *112*, 673–674.

(10) Kitagawa, S.; Kitaura, R.; Noro, S.-i. Functional Porous Coordination Polymers. *Angew. Chem. Int. Ed.* **2004**, *43*, 2334–2375.

(11) Yamabayashi, T.; Atzori, M.; Tesi, L.; Cosquer, G.; Santanni, F.; Boulon, M. E.; Morra, E.; Benci, S.; Torre, R.; Chiesa, M.; Sorace, L.; Sessoli, R.; Yamashita, M. Scaling Up Electronic Spin Qubits into a Three-Dimensional Metal–Organic Framework. *J. Am Chem. Soc.* **2018**, *140*, 12090–12101.

(12) Kitagawa, S. Future porous materials. *Acc. Chem. Res.* **2017**, *50*, 514—-516.

(13) Evans, J. D.; Bon, V.; Senkovska, I.; Lee, H. C.; Kaskel, S. Four-dimensional metal-organic frameworks. *Nat. Commun.* **2020**, *11*, 2690–2701.

(14) Zadrozny, J. M.; Niklas, J.; Poluektov, O. G.; Freedman, D. F. Millisecond coherence time in a tunable molecular electronic spin qubit. *ACS Cent. Sci.* **2015**, *1*, 488–492.

(15) Takahashi, S.; Tupitsyn, I. S.; van Tol, J.; Beedle, C. C.; Hendrickson, D. N.; Stamp, P. C. E. Decoherence in crystals of quantum molecular magnets. *Nature* **2011**, *476*, 76–79.

(16) Wasielewski, M. R. et al. Exploiting chemistry and molecular systems for quantum information science. *Nat. Rev. Chem.* **2020**, *4*, 490–504.

(17) Morris, W.; Volosskiy, B.; Demir, S.; Gándara, F.; McGrier, P. L.; Furukawa, H.; Cascio, D.; Stoddart, J. F.; Yaghi, O. M. Synthesis, Structure, and Metalation of Two New Highly Porous Zirconium Metal–Organic Frameworks. *Inorganic Chemistry* **2012**, *51*, 6443–6445, PMID: 22676251.

(18) Feng, D.; Chung, W.-C.; Wei, Z.; Gu, Z.-Y.; Jiang, H.-L.; Chen, Y.-P.; Darensbourg, D. J.; Zhou, H.-C. Construction of Ultrastable Porphyrin Zr Metalâ€“Organic Frameworks through Linker Elimination. *Journal of the American Chemical Society* **2013**, *135*, 17105–17110, PMID: 24125517.

(19) Cavka, J. H.; Jakobsen, S.; Olsbye, U.; Guillou, N.; Lamberti, C.; Bordiga, S.; Lillerud, K. P. A New Zirconium Inorganic Building Brick Forming Metal Organic Frameworks with Exceptional Stability. *Journal of the American Chemical Society* **2008**, *130*, 13850–13851, PMID: 18817383.

(20) Mondloch, J. E.; Katz, M. J.; Planas, N.; Semrouni, D.; Gagliardi, L.; Hupp, J. T.; Farha, O. K. Are Zr6-based MOFs water stable? Linker hydrolysis vs. capillary-force-driven channel collapse. *Chem. Commun.* **2014**, *50*, 8944–8946.

(21) Liu, X.; Demir, N. K.; Wu, Z.; Li, K. Highly Water-Stable Zirconium Metalâ€“Organic Framework UiO-66 Membranes Supported on Alumina Hollow Fibers for Desalination. *Journal of the American Chemical Society* **2015**, *137*, 6999–7002, PMID: 26023819.

(22) Wu, H.; Chua, Y. S.; Krungleviciute, V.; Tyagi, M.; Chen, P.; Yildirim, T.; Zhou, W. Unusual and Highly Tunable Missing-Linker Defects in Zirconium Metalâ€“Organic Framework UiO-66 and Their Important Effects on Gas Adsorption. *Journal of the American Chemical Society* **2013**, *135*, 10525–10532, PMID: 23808838.

(23) Katz, M. J.; Brown, Z. J.; ColÃ³n, Y. J.; Siu, P. W.; Scheidt, K. A.; Snurr, R. Q.; Hupp, J. T.; Farha, O. K. A facile synthesis of UiO-66, UiO-67 and their derivatives. *Chem. Commun.* **2013**, *49*, 9449–9451.

(24) Urtizberea, A.; Natividad, E.; Alonso, P. J.; Andrés, M. A.; Gascón, I.; Goldmann, M.; Roubeau, O. A Porphyrin Spin Qubit and Its 2D Framework Nanosheets. *Adv. Funct. Mater.* **2018**, *28*, 1801695.

(25) Chen, Z.; Hanna, S. L.; Redfern, L. R.; Alezi, D.; Islamoglu, T.; Farha, O. K. Reticular chemistry in the rational synthesis of functional zirconium cluster-based MOFs. *Coordination Chemistry Reviews* **2019**, *386*, 32–49.

(26) Karadeniz, B.; Žilić, D.; Huskić, I.; Germann, L. S.; Fidelli, A. M.; Muratović, S.; Lončarić, I.; Etter, M.; Dinnebier, R. E.; Barišić, D.; Cindro, N.; Islamoglu, T.; Farha, O. K.; Friščić, T.; Užarević, K. Controlling the Polymorphism and Topology Transformation in Porphyrinic Zirconium Metal–Organic Frameworks via Mechanochemistry. *J. Am. Chem. Soc.* **2019**, *141*, 19214.–19220, PMID: 31747754.

(27) Zadrozny, J. M.; Gallagher, A. T.; Harris, T. D.; Freedman, D. F. A porous array of clock qubits. *JACS* **2017**, *139*, 7089–7094.

(28) Yu, C.-J.; Kugelgen, S. c.; Krzyaniak, M. D.; JI, W.; Dichtel, W. R.; Wasielewski, M. R.; Freedman, D. E. Pin and Phonon Design in Modular arrays of molecular qubits. *Chem. Mater.* **2020**, *32*, 10200–10206.

(29) Richert, S.; Cremers, J.; Anderson, H. L.; Timmel, C. R. Exploring template-bound dinuclear copper porphyrin nanorings

by EPR spectroscopy. *Chem. Sci.* **2016**, *7*, 6952–6960.
(30) Yamabayashi, T.; Atzor, M.; L., T.; Cosquer, G.; Santanni, F.; Boulon, M.-E.; Morra, E.; Benci, R., S. adn Torre; Chiesa, M.; Sorace, L.; Sessoli, R.; Yamashita, M. Scaling Up Electronic Spin Qubits into a Three-Dimensional Metal-Organic Framework. *JACS* **2018**, *140*, 12090–12101.
(31) Stolar, T.; Užarević, K. Mechanochemistry: an efficient and versatile toolbox for synthesis, transformation, and functionalization of porous metal–organic frameworks. *CrystEngComm* **2020**, *22*, 4511–4525.
(32) Martinez, V.; Karadeniz, B.; Biliškov, N.; Lončarić, I.; Muratović, S.; Žilić, D.; Avdoshenko, S. A.; Roslova, M.; Popov, A. A.; Užarević, K. Tunable Fulleretic Sodalite MOFs: Highly Efficient and Controllable Entrapment of C_{60} Fullerene via Mechanochemistry. *Chem. Mater.* **2020**, *32*, 10628–10640.
(33) Mulholland, A. R.; Woodward, C. P.; Langford, S. J. Fullerene-templated synthesis of a cyclic porphyrin trimer using olefin metathesis. *Chem. Commun.* **2011**, *47*, 1494–1496.
(34) Zheng, D.-Y.; Chen, E.-X.; Yeab, C.-R.; Huang, X.-C. High-efficiency photo-oxidation of thioethers over C60@PCN-222 under air. *J.Matter. Chem. A* **2019**, *7*, 22084–22091.
(35) Finazzo, C.; Calle, C.; Stoll, S.; Doorslaer, S.; Schweiger, A. Matrix effects on copper(II)phthalocyanine complexes. A combined continuous wave and pulse EPR and DFT study. *Phys. Chem. Chem. Phys.* **2006**, *8*, 1942–53.
(36) Stoll, S.; Schweiger, A. EasySpin, a comprehensive software package for spectral simulation and analysis in EPR. *J. Magn. Reson.* **2006**, *178*, 42–55.
(37) Basu, P. Use of EPR Spectroscopy in Elucidating Electronic Structures of Paramagnetic Transition Metal Complexes. *J. Chem. Educ.* **2001**, *78*, 666–669.
(38) Cunningham, K. L.; McNett, K. M.; Pierce, R. A.; Davis, K. A.; Harris, H. H.; Falck, D. M.; McMillin, D. R. EPR spectra, luminescence data, and radiationless decay processes of copper(II) porphyrins. *Inorg. Chem.* **1977**, *36*, 608–613.
(39) Gómez-Vidales, V.; Borja-Miranda, A.; Cortez-Maya, S.; Amelines-Sarria, O.; Rivera, M.; Martínez-García, M. Design and synthesis of multi Cu(II)-porphyrin array. *Open Chem. J.* **2016**, *3*, 25–34.
(40) Hoffmann, S. K.; Goslar, J. *Appl. Magn. Reson.* **1998**, *14*, 293–303.
(41) Fielding, A. J.; Fox, S.; Millhauser, G. L.; Chattopadhyay, M.; Kroneck, P. M. H.; Fritz, G.; Eaton, G. R.; Eaton, S. S. *J. Magn. Reson.* **2006**, *179*, 92–104.
(42) Kveder, M.; Merunka, D.; Jokić, M.; Makarević, J.; Rakvin, B. *Phys. Rev. B* **2009**, *80*, 052201–052205.
(43) Makinen, M. W.; Yim, M. B. Coordination environment of the active–site metal ion of liver alcohol dehydrogenase. *Proc. Natl. Acad. Sci.* **1981**, *78*, 6221–6225.
(44) Yu, C.-J.; Krzyaniak, M. D.; Fataftah, M. S.; Wasielewski, M. R.; Freedman, D. E. A concentrated array of copper poprhyrin candidate qubits. *Chem. Sci.* **2019**, *10*, 1702–1708.
(45) Burns, C. S.; Aronoff-Spencer, E.; Dunham, C. M.; Lario, P.; Avdievich, N. I.; Antholine, W. E.; Olmstead, M. M.; Vrielink, A.; Gerfen, G. J.; Peisach, J.; Scott, W. G.; Millhauser, G. L. Molecular Features of the copper binding sites in the octarepeat domain of the prion protein. *Biochemistry* **2002**, *41*, 3991–4001.
(46) Van Doorslaer, S.; Vinck, E. The strength of EPR and ENDORm techniques in revealing structure-function relationships in metalloproteins. *Phys. Chem. Chem. Phys.* **2007**, *9*, 4620–4638.
(47) Silva, K. I.; Michael, B. C.; Geib, S. J.; Saxena, S. ESEEM analysis of multi-histidine Cu(II).coordination in model complexes, peptides, and amyloid-beta. *J. Phys. Chem. B* **2014**, *118*, 8935–8944.
(48) Grimaldi, S.; Arias-Cartin, R.; Lanciano, P.; Lyubenova, S.; Endeward, B.; Prisner, T. F.; Magalon, A.; Guigliarelli, B. Direct Evidence for Nitrogen Ligation to the High Stability Semiquinone Intermediate in Escherichia coli Nitrate Reductase A. *J. Biol. Chem.* **2010**, *285*, 179–187.
(49) Deligiannakis, Y.; Louloudi, M.; Hadjiliadis, N. Electron spin echo envelope modulation (ESEEM) spectroscopy as a tool to investigate the coordination environment of metal centers. *Coordin. Chem. Rev.* **2000**, *204*, 1–112.
(50) Gramza, M.; Hilczer, W.; Goslar, J.; Hoffmann, S. K. Electron spin relaxation and ESEEM spectroscopy of the glycine radical in diglycine nitrate single crystal. *Acta Chem. Scand.* **1997**, *51*, 556–561.
(51) Ling, Y.; Diliën, H.; Vanderzande, D.; Adriaensens, P. J.; Van Doorslaer, S. Electronic structure of the positive radical of 13C-labeled poly(3-octylthienylene vinylene) polymer. *Appl. Magn. Reson.* **2014**, *45*, 827–839.
(52) Zadrozny, J. M.; Gallagher, A. T.; Harris, T. D.; Freedman, D. F. A porous array of clock qubits. *JACS* **2017**, *139*, 7089–7094.